Supporting Information

Corns et al. 10.1073/pnas.1409920111

SI Materials and Methods

Electrophysiology. Outer hair cells (OHCs: $n = 92$) and inner hair cells (IHCs: $n = 30$) mainly from the apical coil of the cochlea of C57B mice of either sex were studied in acutely dissected organs of Corti from postnatal day 4 (P4) to P9, where the day of birth is P0. In a few experiments, CD-1, CBA/Ca, and C3HeB/FeJ mice were also used in combination with C57B mice (mainly in Figs. 1 and 2 and Figs. S2 and S3), with similar results between the different strains. Animals were killed by cervical dislocation, under Schedule 1 in accordance with UK Home Office regulations. Cochleae were dissected in normal extracellular solution (in mM): 135 NaCl, 5.8 KCl, 1.3 $CaCl_2$, 0.9 $MgCl_2$, 0.7 NaH_2PO_4, 5.6 D-glucose, 10 Hepes–NaOH. Sodium pyruvate (2 mM), MEM amino acids solution (50×, without L-glutamine), and MEM vitamins solution (100×) were added from concentrates (Fisher Scientific). The pH was adjusted to 7.5 (osmolality ~308 $mmol \cdot kg^{-1}$). The dissected organs of Corti were transferred to a microscope chamber, immobilized by using a nylon mesh fixed to a stainless steel ring, and continuously perfused with the above extracellular solution. The organs of Corti were observed with an upright microscope (Leica; Nikon), with Nomarski differential interference contrast optics (×63 or ×60 water immersion objectives with an additional up to ×2 magnification and ×16 eyepieces).

Whole-cell patch-clamp recordings were performed at room temperature (22–24 °C) by using an Optopatch (Cairn Research Ltd.) amplifier. Patch pipettes (2–3 MΩ) were coated with surf wax (Mr. Zogs SexWax) to minimize the fast capacitance transient of the patch pipette. The pipette intracellular solution contained (in mM): 106 Cs-glutamate, 20 CsCl, 3 $MgCl_2$, 1 EGTA–CsOH, 5 Na_2ATP, 0.3 Na_2GTP, 5 Hepes–CsOH, 10 Na_2-phosphocreatine (pH 7.3; osmolality ~296 $mmol \cdot kg^{-1}$). In some experiments, 147 mM CsCl was used instead of Cs-glutamate. Some recordings were performed by using different concentrations of the fast Ca^{2+} buffer 1,2-Bis(2-aminophenoxy)ethane-*N*,*N*,*N*′,*N*′-tetraacetic acid (BAPTA; 0.1, 1, 5, and 10 mM: Molecular Probes) instead of 1 mM EGTA (Fluka) in the intracellular solution. The osmolality of the intracellular solution with BAPTA was kept constant by adjusting the concentration of Cs-glutamate. Data acquisition was controlled by pClamp (Molecular Devices) or Asyst (Keithley Instruments) software using Digidata boards (Molecular Devices). Recordings were low-pass filtered at 2.5 kHz (8-pole Bessel) and sampled at 5 kHz. Data analysis was performed by using Origin software (OriginLab). The residual series resistance (R_s) after compensation (60–80%) was 1.49 ± 0.16 MΩ ($n = 117$). The average voltage-clamp time constant (product of R_s and membrane capacitance C_m: 7.2 ± 0.2 pF, $n = 117$) was 9.9 ± 0.9 μs. Membrane potentials were corrected for a liquid junction potential (Cs-glutamate: −11 mV; Cs-Cl: −4 mV) measured between electrode and bath solutions.

The effect of endolymph-like extracellular Ca^{2+}, which has been reported to be between 20 and 40 μM (1, 2), was examined by using a solution containing low Ca^{2+} (40 μM Ca^{2+} obtained by buffering 3.7 mM Ca^{2+} with 4 mM hydroxyethyl ethylenediamine triacetic acid, HEDTA). During the experiments in which different extracellular Ca^{2+} concentrations were used (0.04 and 1.3 mM), the hair bundles were topically superfused, and the fluid jet pipette was also filled with the same solution.

Bundle imaging. To determine whether the fluid-jet stimulation produces a uniform bundle displacement in both OHCs and IHCs (C57B mice, P6–P7), their hair bundles were viewed with a Nikon FN1 microscope with 75× magnification and images captured with a Flash 4.0 SCCD camera (Hamamatsu, Japan). Hair bundles were deflected with the fluid jet in response to excitatory step stimuli, and images were captured at a rate of 400 frames per second (512 × 512 pixels). Hair bundle movements were tracked at three positions (1: left; 2: middle; 3: right) on the same bundle (Fig. S1 *C*–*F*) by using Fiji software (3). Lines were drawn across the stereocilia at these three positions, perpendicular to the direction of bundle motion, and a projected time-based z-stack of the pixels under the line was made (Fig. S1 *E* and *F*, *Left*) (3). Excitatory movement of the stereocilia from their resting position was measured with Photoshop initially as a pixel shift and then converted to nm (290 pixels = 10 μm).

1. Bosher SK, Warren RL (1978) Very low calcium content of cochlear endolymph, an extracellular fluid. *Nature* 273(5661):377–378.
2. Salt AN, Inamura N, Thalmann R, Vora A (1989) Calcium gradients in inner ear endolymph. *Am J Otolaryngol* 10(6):371–375.
3. Schindelin J, et al. (2012) Fiji: An open-source platform for biological-image analysis. *Nat Methods* 9(7):676–682.

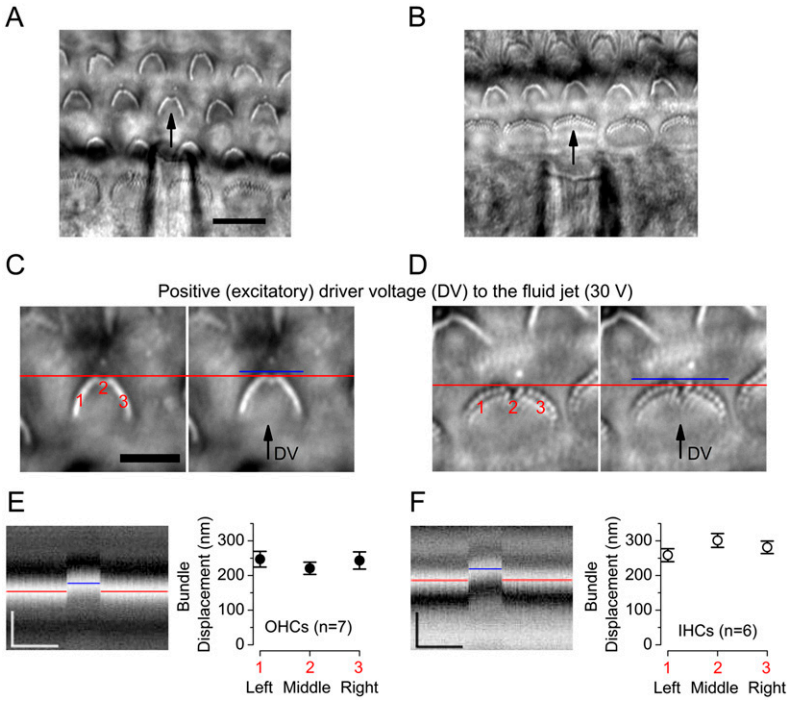

Fig. S1. The fluid-jet stimulation produces a uniform bundle displacement in both OHCs and IHCs. (*A* and *B*) Images showing the relative position of the hair bundle of an OHC (*A*; P7) and an IHC (*B*; P6) and the pipette tip of the fluid jet (see *Materials and Methods* for more details). (Scale bar: 10 μm.) (*C* and *D*) Images of the hair bundle position at rest (*Left*; indicated by the red lines) and during excitatory bundle stimulation (*Right*; indicated by the blue lines) using force-step stimuli in an OHC and an IHC, respectively (for details, see *Materials and Methods*). The numbers (1–3) indicate the positions at which the hair bundle movements were tracked. (Scale bar: 5 μm.) (*E* and *F*) *Left* shows time-based *z*-stack projections of the pixels from the line drawn at position 2 in response to excitatory bundle stimulation, as in *C* and *D*. Again, red lines indicate the resting position of the stereocilia, and the blue is the excitatory displacement. (Scale bars: *y* axis, 1 μm; *x* axis, 100 ms.) *Right* shows the average excitatory displacement of stereocilia from OHCs ($n = 7$) and IHCs ($n = 6$) measured in the three bundle locations shown in *C* and *D*: 1, left; 2, middle; 3, right. Note that bundle motion during fluid-jet stimulation was not significantly different among the three positions along the bundle width of both OHCs (one-way ANOVA: $P = 0.31$) and IHCs ($P = 0.73$); post tests were not calculated because $P > 0.05$. This result indicates that our fluid jet produces a uniform displacement of bundles.

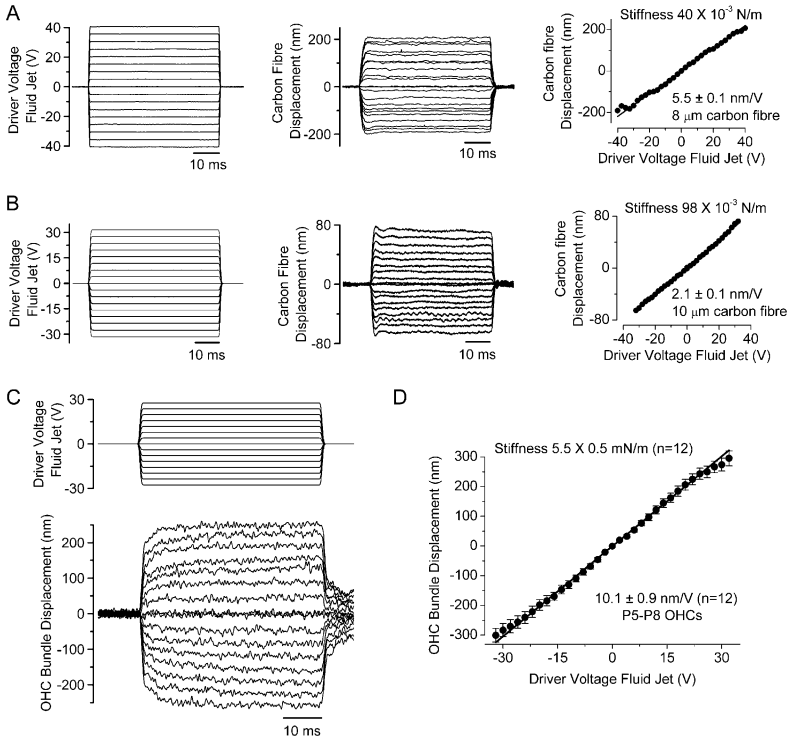

Fig. S2. Calibration of the fluid jet and hair bundle movement. (*A* and *B*) Driver voltage to the fluid jet (*Left*), carbon fiber displacement (*Center*) measured at ~2 mm from the tip and the relation between the two (*Right*) for two different fluid jets and fibers with a diameter of 8 μm (*A*) and 10 μm (*B*). The stiffness of the fibers (shown above *Right*) was measured by hanging an electron microscope copper grid of known mass (0.3 mg) at ~2 mm from its tip and measuring the deflection due to gravity (1). The fiber stiffness and the fluid-jet–induced displacement were measured at approximately the same place along the fiber. The carbon fibers were positioned perpendicular to the tip of the fluid jet pipette. Continuous lines are from a linear fit, and values are indicated. Note that the carbon fiber displacement traces, which provide an indication of the force/pressure exerted by the jet, remain constant during a step stimulus. (*C*) Example of bundle displacement recordings from a P5 OHC. (*D*) Steady-state bundle displacement and driver voltage to the fluid jet relation from P5–P8 OHCs ($n = 12$). The linear fit value (10.1 nm/V) was used to transform the driver voltages to the fluid jet into nanometer bundle displacements for OHCs. The linear relationship between bundle displacement and driver voltages implies that there is no obvious contribution of the gating compliance to the bundle movements (2), probably because the pivotal stiffness of the mammalian hair bundle is relatively large (see also ref. 3). The average steady stiffness of the OHC bundles (shown above the trace) was calculated as described (3) using the force from the fluid jet applied to the OHC bundle from the 10-μm–diameter carbon fibers (*Materials and Methods*) and the bundle movement (volts per nanometer). The size and shape of the fluid jet pipette used for these experiments was similar to those used when mechanoelectrical transducer (MET) currents were recorded in isolation.

1. Kros CJ, Rüsch A, Richardson GP (1992) Mechano-electrical transducer currents in hair cells of the cultured neonatal mouse cochlea. *Proc Biol Sci* 249(1325):185–193.
2. Howard J, Hudspeth AJ (1988) Compliance of the hair bundle associated with gating of mechanoelectrical transduction channels in the bullfrog's saccular hair cell. *Neuron* 1(3):189–199.
3. Géléoc GSG, Lennan GWT, Richardson GP, Kros CJ (1997) A quantitative comparison of mechanoelectrical transduction in vestibular and auditory hair cells of neonatal mice. *Proc Biol Sci* 264(1381):611–621.

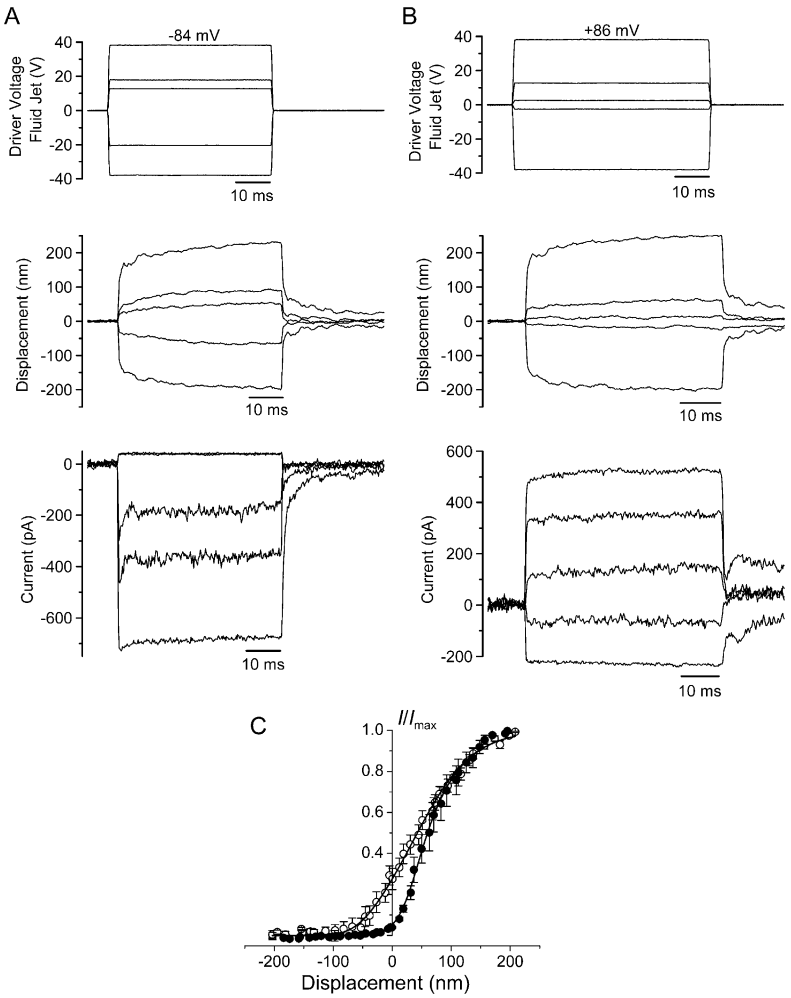

Fig. S3. MET currents and bundle displacements recorded simultaneously in OHCs. (*A* and *B*) Driver voltages to the fluid jet (*Top*), bundle displacement at the tip of the hair bundle (*Middle*), and transducer currents recorded at −84 and +86 mV (*Bottom*) from a P4 OHC. Note that the holding current was zeroed and was −111 pA at −84 mV and +562 pA at +86 mV. At −84 mV (*A*), positive driver voltages and displacements (excitatory direction) elicited inward (negative) transducer currents that declined or adapted over time, which was evident for the intermediate (nonsaturating) bundle displacements. A small transducer current was present at rest (before $t = 0$), and inhibitory bundle displacement turned this current off. Note that the current decline for intermediate stimulation was not associated with any relaxing back of the bundle toward the resting position (see also Fig. S2), indicating that the adaptation is an intrinsic property of the transduction apparatus and not an artifact of the fluid-jet stimulation. In addition, we found that after a rapid initial response to the step, the bundle exhibits a slow movement further away from the resting position, as shown (1–3). This finding is an intrinsic feature of the bundles attributed to the hydrodynamics within the bundle (1) because it is not observed when stimulating a carbon fiber with the jet (Fig. S2). At +86 mV (*B*), excitatory bundle displacements elicited outward (positive) currents with no signs of adaptation. A larger fraction of the current was activated at rest. (*C*) Normalized peak transducer current as a function of bundle displacement for six OHCs (P4–P5). The resting open probability between −81 mV (0.040 ± 0.004; $n = 6$) and +99 mV (0.293 ± 0.005) was significantly different ($P < 0.0005$). Fits to the data points were obtained by using Eq. **2** (Fig. 1 legend). At −84 mV, $I_{max} = -511$ pA, $a_1 = 0.044$ nm^{-1}, $a_2 = 0.021$ nm^{-1}, x_1 and $x_2 = 42$ nm; at +86 mV, $I_{max} = 458$ pA, and the other parameters were as at −84 mV, except $x_1 = -56$ nm, indicating a leftward shift of 98 nm upon depolarization. The shape change in the current-displacement relation, which is fitted with second-order Boltzmann functions, implies that the MET channel has two closed states and one open state [turtle (4); mouse (1, 3)] and has been interpreted as being due to the set point of the transition between the two closed states being voltage-sensitive (and hence Ca^{2+}-sensitive), but not that of the opening transition (4).

1. Géléoc GSG, Lennan GWT, Richardson GP, Kros CJ (1997) A quantitative comparison of mechanoelectrical transduction in vestibular and auditory hair cells of neonatal mice. *Proc Biol Sci* 264(1381):611–621.
2. Kros CJ, Lennan GWT, Richardson GP (1995) Transducer currents and bundle movements in outer hair cells of neonatal mice. *Active hearing*, ed Flock Å (Elsevier, Oxford), pp 113–125.
3. Kros CJ, et al. (2002) Reduced climbing and increased slipping adaptation in cochlear hair cells of mice with Myo7a mutations. *Nat Neurosci* 5(1):41–47.
4. Crawford AC, Evans MG, Fettiplace R (1989) Activation and adaptation of transducer currents in turtle hair cells. *J Physiol* 419:405–434.

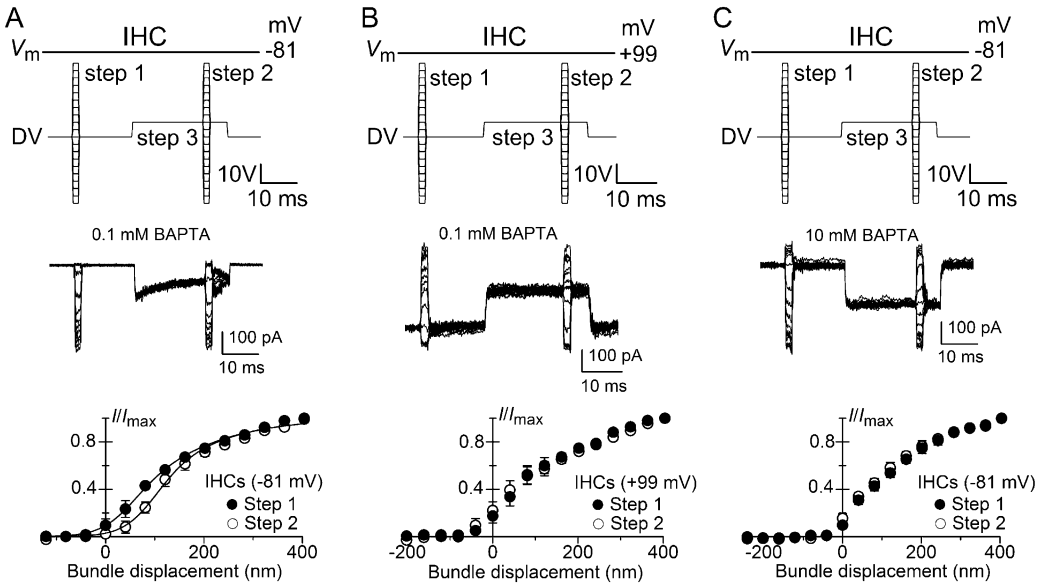

Fig. S4. Adaptive shift in a paired-pulse protocol applied to IHCs is abolished by strong Ca^{2+} buffering and depolarization. MET currents (*Middle*) were recorded from IHCs in response to paired-pulse stimulation with an 81-nm adaptive step (*Upper*), as described for OHCs in Fig. 4. MET currents recorded in P7 IHCs at −81 mV (*A*) and +99 mV (*B*) in the presence of 0.1 mM and at −81 mV in 10 mM intracellular BAPTA (*C*). *Lower* shows the normalized peak MET current recorded in P7 IHCs before (step 1) and during (step 2) the adaptive step (step 3) as a function of bundle displacement in 0.1 mM intracellular BAPTA (*A* and *B*; $n = 4$) and 10 mM BAPTA (*C*; $n = 4$). Data points in *A* were fitted by using Eq. **2**: step 1, $I_{max} = -419$ pA, $a_1 = 0.023$ nm^{-1}, $a_2 = 0.0089$ nm^{-1}, x_1 and $x_2 = 64$ nm; step 2, $I_{max} = -401$ pA, other parameters were as for step 1, except for $x_1 = 122$ nm, indicative of a Ca^{2+}-dependent adaptive shift of 58 nm to the right, in agreement with previous findings in turtle hair cells (1). The bundle displacement at which 50% of the maximum MET current is activated was significantly different between step 1 (103.3 ± 8.6 nm; $n = 3$) and step 2 (130.0 ± 12.5 nm; $n = 3$) in 0.1 mM BAPTA and at −81 mV (*A*; paired *t* test: $P < 0.05$). No significant difference was found in any of the other experimental conditions (*B*: step 1, 85.6 ± 23.3 nm, $n = 3$; step 2, 81.2 ± 28.2 nm; *C*: step 1, 100.3 ± 11.8 nm, $n = 4$; step 2, 106.6 ± 13.6 nm). The conversion value used to express the piezo driver voltage into displacement (*Bottom*) was the same as that used for OHCs (Fig. S2 *C* and *D*) as the bundle displacements for a given driver voltage were similar between the two cell types (Fig. S1 *E* and *F*).

1. Crawford AC, Evans MG, Fettiplace R (1989) Activation and adaptation of transducer currents in turtle hair cells. *J Physiol* 419:405–434.